

Nonlinear control of a 3-DOF robotic arm driven by electro-pneumatic servo systems

Duc Thinh Le¹, Van Trong Dang¹, Viet Hung Pham¹, Van Anh Nguyen Thi¹, Danh Huy Nguyen¹, Duc Truong Vu² and Tung Lam Nguyen¹

¹Hanoi University of Science and Technology

²Le Quy Don Technical University

*Corresponding author E-mails: huy.nguyendanh@hust.edu.vn and lam.nguyentung@hust.edu.vn

Abstract

The paper proposes an effective control approach to a 3-DOF serial robotic arm actuated by electro-pneumatic servo systems (EPSS). The robot control problem is divided into robot dynamics and pneumatic actuators sub-systems, and the control is subsequently elaborated for each sub-system. The challenging task arises when dealing with pneumatic systems where system parametric information is very difficult to acquired correctly. Hence, the Lyapunov-based control is formulated to derive the control signal in presence of external disturbances and model uncertainties thank to the integrated disturbance observer. The closed-loop system stability is analytically proven through a series of Lyapunov candidate functions. Simulations using MATLAB/Simscape Multibody Link plug-in on Solidworks are carried out to demonstrate the control validity.

Keywords: Backstepping Sliding Mode Control (BSMC), 3-DOF robotic arm, electro-pneumatic servo system, nonlinear disturbance observer.

Symbols

Symbols	Units	Description
m_1	kg	Upper arm mass with cylinder
m_2	kg	Forearm mass
m_f	kg	Load mass with translation joint cylinder
I_1	kg · m ²	Moment of inertia for upper arm around the shoulder
I_2	kg · m ²	Moment of inertia for forearm around the elbow
P_1P_2	m	Upper arm length
P_1P_{m1}	m	Distance from centroid of upper arm to shoulder
P_2P_{m2}	m	Distance from centroid of forearm to elbow
θ_1	rad	Upper arm rotation range
θ_2	rad	Forearm rotation range

Abbreviations

PRA	Pneumatic Robotic Arm
EPSS	Electro-Pneumatic Servo System
DOF	Degree of Freedom
NDO	Nonlinear Disturbance Observer

Tóm tắt

Bài báo trình bày phương án điều khiển robot 3 bậc tự do được truyền động bằng khí nén. Bài toán điều khiển được chia nhỏ thành hai bài toán con bao gồm động lực học robot và cơ cấu chấp hành khí nén, dựa vào đó, bộ điều khiển được thiết kế trên các hệ con. Những thách thức khi điều khiển đến từ việc khó khăn trong việc đo lường, xác định tham số của hệ thống truyền động khí nén. Trong bài báo này, bộ điều khiển được thiết kế dựa trên lý thuyết ổn định Lyapunov có tích hợp bộ quan sát nhiễu dùng để ước lượng tham số bất định cũng như nhiễu tác động lên đối tượng. Tính ổn định của hệ thống kín được chứng minh và các kết quả mô phỏng cho thấy hiệu quả của phương pháp đề xuất.

1. Introduction

In recent years, advances in technologies facilitate many industrial automation processes. This creates an increasing demand for actuators driven in high speed for the purpose of reducing time consumption in industrial tasks like assembly process. In comparison with servo motors, electro-pneumatic servo systems (EPSS) offer better characteristics such as low cost, high power-to-weight ratio, the absence of magnetic field and simple cleaning and maintenance. These distinctive advantages allow pneumatic-driven units to be integrated in a wide range of industrial actuators. Therefore, the problems of exact control of this kind of actuators are necessary. However, many hindrances

in model analyzing and controlling are found such as the comprehensibility of air and adverse effects of driving pneumatic components in high speed that are oscillatory behaviours and parasitic moving frictions [1].

The past decades also witnessed the profound automation in many industries by the popularity of manipulators. Indeed, the use of industrial manipulators improves the overall productivity and reduces human error, as they have a superior load-lifting capability and can replace human labor in dangerous environments. They perform procedures repeatedly with high precision and are widely used from welding robots to car assembly lines. Generally, manipulator joints are driven in different modes, i.e., full-actuated [2] and under-actuated [3]. It is more challenging to do the under-actuated ones, since both kinematic and dynamic constraints are tied in an under-actuated motion system. Therefore, it is inappropriate to apply directly conventional Euler–Lagrange method to this kind of joints. Thus, complexity [4] and uncertainty of the model also degrade the controller robustness. One typical model of a manipulator is from [5, 6]. It is a 2-DOF robotic manipulator is comprised of an upper arm, a forearm, a disc load, and a fixed torso. The shoulder and elbow joints are driven to rotate by two Electrohydraulic actuators (EHAs). In this paper, we propose a model using EPSS with additional electro-pneumatic servo actuator at the end of the forearm, which governs the extension of the forearm and makes our model 3-DOF, providing a better range of work and applications. The 3D model of this manipulator is illustrated in Figure 1.

Due to the enormous applicability of pneumatic units in industries, researchers have come up with different strategies to control accurately this type of actuator [7]. An active rejection-disturbance controller (ARDC) was utilized in [8] and [9] and brought promising results. Pulse-width modulation technique and fuzzy logic controller were combined in [10] to control an electro-pneumatic servo systems. In [11], Karpenko et al. proposed a quantitative feedback theory of a PI controller for positioning of a servo-pneumatic servo actuator. Paper [12] presented a hybrid controller of fuzzy controller and PID controller. These linear control schemes experienced difficulties in obtaining both fast response and precise position control at the same time, due to the nonlinear nature of the EPSS.

Therefore, different approaches are implemented to tackle this problem. Popular employed methods can be listed as backstepping technique and Sliding Mode Control (SMC). Tracking position control of EPSS is concerned in [13] with a backstepping controller. In [14], authors applied adaptive backstepping controller using Nussbaum gain with unknown model. A different approach of adaptive backstepping control is implemented in [15]. For SMC, it showed a wider range of application in a lot of control scenarios: SMC for servo-pneumatic servo system [16] and [17], SMC with friction compensation [18], SMC with Particle Swarm Optimization [19], and adaptive SMC [20]. These papers proved the robustness and efficiency of SMC for a highly non-linear model like pneumatic system. Some authors also combined these techniques together and obtained even remarkably better control quality like Ren et al. [21] and Lu et al. [22]. SMC algorithms in these mentioned papers were found to be effective against external disturbances with addition of an observer like extended state observer (ESO).

In this paper, a new control approach using Backstepping-Sliding Mode Control (BSMC) and nonlinear high-gain dis-

turbance observer is presented to the 3-DOF pneumatic-driven manipulator. BSMC is used in control the dynamics of the EPAs and the kinematics of the entire manipulator itself. The manipulator model under the effect of external disturbances are also considered. The novel contributions of this paper are summarized as follows:

- (i). The 3-DOF robotic arm driven by EPSS including shoulder, elbow, and translational joint is built, in which the 3-DOF manipulator is designed in CAD and a 3D model with precise parameters of the model is built in Solidworks and Simscape Multibody to validate the model in 3D simulation.
- (ii). The nonlinear high-gain disturbance observer is embedded with BSMC to have robust property against external disturbances affecting on the manipulator. The stability of the controller is proved mathematically by Lyapunov stability theory. The performance of the BSMC with nonlinear high-gain disturbance observer is compared to the conventional BSMC using saturation function.

The reminder of this article is organized as follows: the Section 1 is introduction, and the Section 2 concerns about mathematical model of the manipulator. SMC with nonlinear high-gain DOB is proposed in Section 3, followed by the simulation evaluation in Section 4. Finally, Section 5 discusses the simulation results and future development.

2. Mathematical modeling of the 3-DOF PRA

2.1. Dynamic and kinematic model of robotic arm

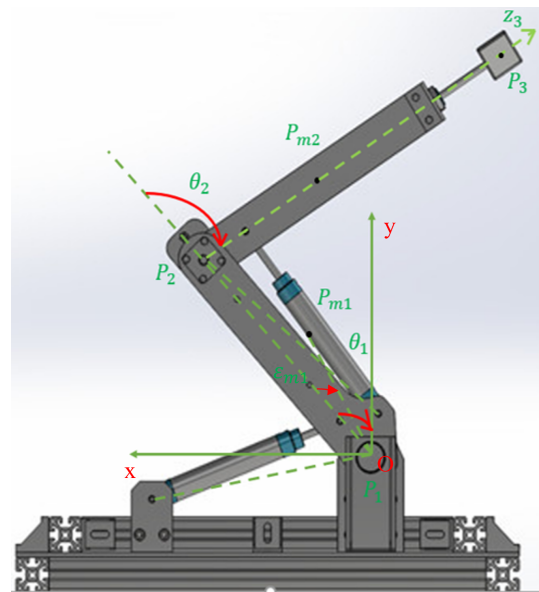


Figure 1: The 3-DOF pneumatic robotic arm configuration.

The 3-DOF pneumatic robotic arm is shown in Figure 1, in which the shoulder, elbow, and translational joints are driven by three independent single-rod cylinder electro-pneumatic servo actuators. The robot position vectors P_{m1} , P_{m2} , and P_3 are given by, respectively:

$$\mathbf{r}_{P_{m1}/O} = \begin{bmatrix} -P_1 P_{m1} \sin(\theta_1 + \epsilon_{m1}) \\ P_1 P_{m1} \cos(\theta_1 + \epsilon_{m1}) \end{bmatrix} \quad (1)$$

$$\mathbf{r}_{P_{m2}/O} = \begin{bmatrix} -P_1 P_2 \sin(\theta_1) - P_2 P_{2m} \sin(\theta_1 + \theta_2) \\ P_1 P_2 \cos(\theta_1) + P_2 P_{2m} \cos(\theta_1 + \theta_2) \end{bmatrix} \quad (2)$$

$$\mathbf{r}_{P3} = \begin{bmatrix} -P_1 P_2 \sin(\theta_1) - z_3 \sin(\theta_1 + \theta_2) \\ P_1 P_2 \cos(\theta_1) + z_3 \cos(\theta_1 + \theta_2) \end{bmatrix} \quad (3)$$

It is straightforward to determine the velocity vectors P_{m1} , P_{m2} , and P_3 as follows:

$$\mathbf{v}_{P_{m1}/O} = \begin{bmatrix} -P_1 P_{m1} \dot{\theta}_1 C(\theta_1 + \varepsilon_{m1}) \\ -P_1 P_{m1} \dot{\theta}_1 S(\theta_1 + \varepsilon_{m1}) \end{bmatrix} \quad (4)$$

$$\mathbf{v}_{P_{m2}/O} = \begin{bmatrix} -P_1 P_2 \dot{\theta}_1 C(\theta_1) - P_2 P_{2m} (\dot{\theta}_1 + \dot{\theta}_2) C(\theta_1 + \theta_2) \\ -P_1 P_2 \dot{\theta}_1 S(\theta_1) - P_2 P_{2m} (\dot{\theta}_1 + \dot{\theta}_2) S(\theta_1 + \theta_2) \end{bmatrix} \quad (5)$$

$\mathbf{v}_{P3} =$

$$\begin{bmatrix} P_1 P_2 \dot{\theta}_1 C(\theta_1) - z_3 (\dot{\theta}_1 + \dot{\theta}_2) C(\theta_1 + \theta_2) - \dot{z}_3 S(\theta_1 + \theta_2) \\ -P_1 P_2 \dot{\theta}_1 S(\theta_1) - z_3 (\dot{\theta}_1 + \dot{\theta}_2) S(\theta_1 + \theta_2) + \dot{z}_3 C(\theta_1 + \theta_2) \end{bmatrix} \quad (6)$$

where $S(\cdot)$ and $C(\cdot)$ denote $\sin(\cdot)$ and $\cos(\cdot)$, respectively. From the system representation, the total kinetic energy K of the 3-DOF PRA including the cylinders and the load mass is computed as follows:

$$\begin{aligned} K &= K_1 + K_2 \\ &= \frac{1}{2} m_1 (P_1 P_{m1} \dot{\theta}_1)^2 + \frac{1}{2} I_1 \dot{\theta}_1^2 + \frac{1}{2} m_2 v_{P_{m2}/O}^T v_{P_{m2}/O} \\ &\quad + \frac{1}{2} I_2 f (\dot{\theta}_1 + \dot{\theta}_2)^2 + \frac{1}{2} m_f v_{mf}^T v_{mf} \end{aligned} \quad (7)$$

where K_1 and K_2 denote the kinetic energy of the the upper arm and the forearm, respectively. Similarly, the total gravitational potential energy of the 3-DOF PRA including the cylinders and the load mass is computed by:

$$\begin{aligned} U &= U_1 + U_2 + U_f \\ &= m_1 g P_1 P_{m1} \cos(\theta_1 + \varepsilon_{m1}) \\ &\quad + m_2 g (P_1 P_2 \cos(\theta_1) + P_2 P_{2m} \cos(\theta_1 + \theta_2)) \\ &\quad + m_f g (P_1 P_2 \cos(\theta_1) + z_3 \cos(\theta_1 + \theta_2)) \end{aligned} \quad (8)$$

where U_1 , U_2 , and U_f are the gravitational potential energy of the upper arm, the forearm, and the translational joint. g denotes the gravitational acceleration. Then, the total energy E of the three-link robotic arm system is given by:

$$E = K_1 + K_2 - U_1 - U_2 - U_f \quad (9)$$

By using simple geometric calculations, three cylinder dynamic lengths c_1 , c_2 , c_3 are represented by:

$$\begin{aligned} c_1 &= \sqrt{a_1^2 + b_1^2 - 2a_1 b_1 \cos\left(\frac{\pi}{2} - \theta_1 + \varepsilon_{11}\right)} \\ c_2 &= \sqrt{a_2^2 + b_2^2 - 2a_2 b_2 \cos(\pi - \theta_2 - \varepsilon_{21})} \\ c_3 &= x_3 \end{aligned} \quad (10)$$

Define the generalized force vectors T including torques T_1 , T_2 and force F_3 as:

$$\mathbf{T} = [T_1 \ T_2 \ T_3]^T \quad (11)$$

where $T_1 = F_1 L_1$, $T_2 = F_2 L_2$, $T_3 = F_3$; L_1, L_2 are the two dynamic force arms, given as:

$$\begin{aligned} L_1 &= a_1 \sin\left(\arccos\left(\frac{a_1^2 + c_1^2 - b_1^2}{2a_1 c_1}\right)\right) \\ L_2 &= a_2 \sin\left(\arccos\left(\frac{a_2^2 + c_2^2 - b_2^2}{2a_2 c_2}\right)\right) \end{aligned} \quad (12)$$

Choosing the generalized coordinates vector \mathbf{q} :

$$\mathbf{q} = [\theta_1 \ \theta_2 \ z_3]^T \quad (13)$$

The Lagrange equation of the three-DOF robotic arm system is computed as:

$$\mathbf{T} = \frac{\partial}{\partial t} \frac{\partial E}{\partial \dot{\mathbf{q}}} - \frac{\partial E}{\partial \mathbf{q}} \quad (14)$$

Applying the Lagrange equation, then the kinetic equation of the three-link robotic arm system is obtained as follows:

$$\mathbf{M}(\mathbf{q}, \dot{\mathbf{q}}) \ddot{\mathbf{q}} + \mathbf{C}(\mathbf{q}, \dot{\mathbf{q}}) \dot{\mathbf{q}} + \mathbf{G} = \mathbf{T} \quad (15)$$

where

$$\mathbf{M}(\mathbf{q}, \dot{\mathbf{q}}) = \begin{bmatrix} M_{11} & M_{12} & M_{13} \\ M_{21} & M_{22} & M_{23} \\ M_{31} & M_{32} & M_{33} \end{bmatrix}$$

$$\mathbf{C}(\mathbf{q}, \dot{\mathbf{q}}) = \begin{bmatrix} C_{11} & C_{12} & C_{13} \\ C_{21} & C_{22} & C_{23} \\ C_{31} & C_{32} & C_{33} \end{bmatrix}$$

$$\mathbf{G} = \begin{bmatrix} G_1 \\ G_2 \\ G_3 \end{bmatrix}$$

$$\begin{aligned} M_{11} &= I_1 + I_2 + m_1 P_1 P_{1m}^2 + m_2 P_2 P_{m20}^2 + m_f x_3^2 \\ &\quad + m_2 P_1 P_2^2 + m_f P_1 P_2^2 + 2m_2 P_1 P_2 \cdot P_2 P_{m20} \cos \theta_2 \\ &\quad + 2m_f P_1 P_2 \cdot x_3 \cos \theta_2 \end{aligned}$$

$$\begin{aligned} M_{12} &= M_{21} \\ &= I_2 + m_2 P_2 P_{m20}^2 + m_f x_3^2 + m_2 P_1 P_2 \cdot P_2 P_{m20} \cos \theta_2 \\ &\quad + m_f P_1 P_2 \cdot x_3 \cos \theta_2 \end{aligned}$$

$$\begin{aligned} M_{13} &= M_{31} \\ &= m_f P_1 P_2 \sin \theta_2 \end{aligned}$$

$$M_{22} = I_2 + m_2 P_2 P_{m20}^2 + m_f x_3^2$$

$$M_{23} = M_{32} = 0$$

$$M_{33} = m_f$$

$$C_{11} = 0$$

$$\begin{aligned} C_{12} &= m_1 P_1 P_2 \cdot \dot{x}_3 \cos \theta_2 - 2m_2 P_1 P_2 \cdot P_2 P_{m20} \dot{\theta}_1 \sin \theta_2 \\ &\quad - m_2 P_1 P_2 \cdot P_2 P_{m20} \dot{\theta}_2 \sin \theta_2 - 2m_f P_1 P_2 \cdot x_3 \dot{\theta}_1 \sin \theta_2 \\ &\quad - m_f P_1 P_2 \cdot x_3 \dot{\theta}_2 \sin \theta_2 \end{aligned}$$

$$C_{13} = 2m_f x_3 \dot{\theta}_1 + 2m_f x_3 \dot{\theta}_2 + 2m_f P_1 P_2 \cdot \dot{\theta}_1 \cos \theta_2$$

$$C_{21} = 0$$

$$C_{22} = -m_2 P_1 P_2 \cdot P_2 P_{m20} \dot{\theta}_1 \sin \theta_2 - m_f P_1 P_2 \cdot x_3 \dot{\theta}_1 \sin \theta_2$$

$$C_{23} = 2m_f x_3 \dot{\theta}_1 + 2m_f x_3 \dot{\theta}_2 + m_f P_1 P_2 \cdot \dot{\theta}_1 \cos \theta_2$$

$$C_{31} = 0$$

$$C_{32} = m_f P_1 P_2 \cdot \dot{\theta}_1 \cos \theta_2$$

$$C_{33} = 0$$

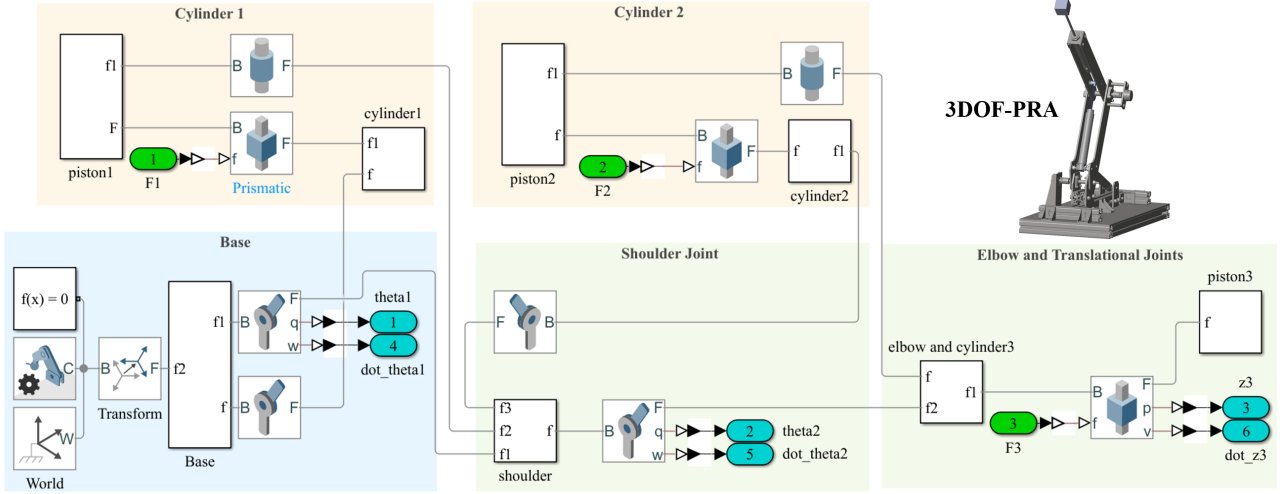


Figure 2: The quasi-physical model of the 3DOF-PRA based on Simscape Multibody.

$$\begin{aligned}
 G1 &= -m_1 g P_1 P_{m1} \sin(\theta_1 + \varepsilon_{11}) \\
 &\quad + m_2 g (P_1 P_2 \sin(\theta_1 + \varepsilon_{11}) + P_2 P_{m2} \sin(\theta_1 + \theta_2)) \\
 &\quad - m_f g (P_1 P_2 \sin(\theta_1 + \varepsilon_{11}) + x_3 \sin(\theta_1 + \theta_2)) \\
 G2 &= m_2 g \cdot P_2 P_{m2} \sin(\theta_1 + \theta_2) - m_f g x_3 \sin(\theta_1 + \theta_2) \\
 G3 &= m_f g \cos(\theta_1 + \theta_2)
 \end{aligned}$$

The matrix $\mathbf{M}(\mathbf{q}, \dot{\mathbf{q}})$ is positive definite and symmetric for all \mathbf{q} . Define state variables for the robotic arm $\mathbf{x}_1 = \mathbf{q}$, then Equation (15) can be rewritten as follows:

$$\begin{cases} \dot{\mathbf{x}}_1 = \mathbf{x}_2 \\ \dot{\mathbf{x}}_2 = \mathbf{M}^{-1}(\mathbf{T} - \mathbf{C}\mathbf{x}_2 - \mathbf{G}) \end{cases} \quad (16)$$

Let $\mathbf{g}_2(\mathbf{q}) = \mathbf{M}^{-1}$ and $\mathbf{f}_2(\mathbf{q}) = -\mathbf{M}^{-1}(\mathbf{C}\mathbf{x}_2 + \mathbf{G})$, Equation (16) is obtained:

$$\begin{cases} \dot{\mathbf{x}}_1 = \mathbf{x}_2 \\ \dot{\mathbf{x}}_2 = \mathbf{f}_2(\mathbf{q}) + \mathbf{g}_2(\mathbf{q})\mathbf{T} \end{cases} \quad (17)$$

2.2. Inverse kinematic model of 3-DOF robotic arm

The goal of the 3-DOF robotic arm system is to control the position of the robot's final action. In order to obtain this, from the position of the last action, the value of 2 rotation angles θ_1, θ_2 and the displacement z_3 of three robotic joints are designed as follows.

The position vector of the robot's last action is defined as:

$$\mathbf{P} = [p_x \quad p_y]^T \quad (18)$$

Then from Figure 1, it can be shown that :

$$p_x^2 + p_y^2 = P_1 P_2^2 + z_3^2 + 2P_1 P_2 z_3 \cos(\theta_2), \quad (19)$$

$$\cos(\theta_2) = \frac{p_x^2 + p_y^2 - P_1 P_2^2 - z_3^2}{2P_1 P_2 z_3}. \quad (20)$$

The rotation angles θ_1 and θ_2 of the robotic arm are calculated as follows:

$$\begin{cases} \theta_1 = \text{ATAN2}(p_y, p_x) - \text{ATAN2}(z_3 \sin \theta_2, P_1 P_2 + z_3 \cos \theta_2) \\ \theta_2 = \text{ATAN2}(\sin \theta_2, \cos \theta_2). \end{cases} \quad (21)$$

2.3. Dynamic model of the EPSS

The quasi-physical model of the 3DOF-PRA based on Simscape Multibody is shown in Fig. 2. The force acting on each robot joint is driven by the pneumatic cylinder actuator. The pneumatic cylinders used to drive the three joints of the robot are assumed to have exactly the same physical structure, thus the dynamic model of cylinders are represented in general as shown in Figure 3.

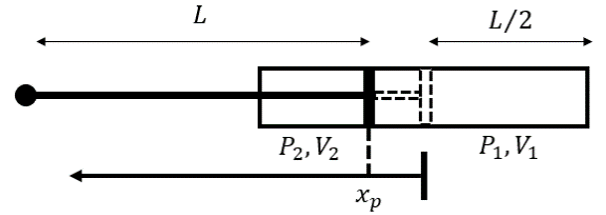


Figure 3: Schematic of the pneumatic cylinder.

The length of the cylinder c is calculated by:

$$c = 3L/2 + x_p \quad (22)$$

where x_p is the piston position, L denotes the piston stroke. The force of the piston, which is caused by the pressure difference between two chambers of the cylinder, is given by:

$$F_a = P_1 A_1 - P_2 A_2 - P_{atm}(A_1 - A_2) \quad (23)$$

where A_1 and A_2 denote the piston effective areas. P_{atm} , P_1 , and P_2 are the absolute pressures of the ambience, the actuator chamber 1, and the chamber 2, respectively. The control valve in the EPSS is a 5/3-way proportional valve, thus the relationship between the control signals $A_{v,i}$ ($i = 1, 2$) is:

$$A_{v,1} = -A_{v,2} = A_v \quad (24)$$

Mass flows entering and leaving of the two cylinder chambers are expressed by:

$$\begin{aligned}
 \dot{\mu}_i(P_u, P_d) &= A_v \psi_i(P_u, P_d) \\
 &= A_v \begin{cases} \frac{C_d P_u C_1}{\sqrt{T}}, \frac{P_d}{P_u} \leq P_{cr} \\ \frac{C_d P_u C_1}{\sqrt{T}} \sqrt{1 - \left(\frac{P_d - P_{cr}}{1 - P_{cr}}\right)^2}, \frac{P_d}{P_u} > P_{cr} \end{cases} \quad (25)
 \end{aligned}$$

where

$$C_1 = \sqrt{\frac{\gamma}{R} \left(\frac{2}{\gamma+1} \right)^{(\gamma+1)(\gamma-1)}} \quad (26)$$

$$\Psi_1 = \begin{cases} \Psi(P_s, P_1), & \text{if } A_v \geq 0 \\ \Psi(P_1, P_{atm}), & \text{if } A_v < 0 \end{cases} \quad (27)$$

$$\Psi_2 = \begin{cases} \Psi(P_2, P_{atm}), & \text{if } A_v \geq 0 \\ \Psi(P_s, P_2), & \text{if } A_v < 0 \end{cases} \quad (28)$$

P_u , P_d , and P_s are the upstream pressure, the downstream pressure, and the supply pressure, T is the upstream temperature of air, P_{cr} is the critical pressure ratio, γ is the ratio of specific heats, C_d is the discharge coefficient, R is the gas constant. The pressure dynamics of the cylinder can be given as:

$$\dot{P}_1 = \frac{\gamma RT}{V_1} \dot{\mu}_1 - \alpha \frac{\gamma P_1 A_1}{V_1} \dot{x}_p \quad (29)$$

$$\dot{P}_2 = \frac{\gamma RT}{V_2} \dot{\mu}_2 + \alpha \frac{\gamma P_2 A_2}{V_2} \dot{x}_p \quad (30)$$

The volumes of two cylinder chamber can be calculated by:

$$\begin{aligned} V_1 &= V_{01} + A_1 \left(\frac{L}{2} + x_p \right) \\ V_2 &= V_{02} + A_2 \left(\frac{L}{2} + x_p \right) \end{aligned} \quad (31)$$

Control valve servo input u is given by:

$$A_v = wk_v u \quad (32)$$

where w denotes valve orifice area gradient, k_v is valve spool position gain. From Equation (22) to (32), the force dynamics of the pneumatic piston is obtained as follows:

$$\dot{F}_a = -\alpha \gamma \dot{x}_p \left(\frac{P_1 A_1^2}{V_1} - \frac{P_2 A_2^2}{V_2} \right) + \gamma RT \left(\frac{A_1 \Psi_1}{V_1} - \frac{A_2 \Psi_2}{V_2} \right) wk_v u \quad (33)$$

Let

$$\mathbf{x} = [x_p \quad \dot{x}_p]^T \quad (34)$$

Then, Equation (33) can be rewritten as:

$$\dot{F}_a = f_a(\mathbf{x}, t) + g_a(\mathbf{x}, t) u \quad (35)$$

where

$$\begin{aligned} f_a(\mathbf{x}, t) &= -\alpha \gamma \dot{x}_p \left(\frac{P_1 A_1^2}{V_1} - \frac{P_2 A_2^2}{V_2} \right) \\ g_a(\mathbf{x}, t) &= \gamma RT \left(\frac{A_1 \Psi_1}{V_1} - \frac{A_2 \Psi_2}{V_2} \right) wk_v \end{aligned} \quad (36)$$

In this paper, we assume that all the EPSS are identical.

3. Proposed approach

3.1. Nonlinear high-gain disturbance observer

Parameter uncertainties and unknown disturbances are always present in the 3-DOF robotic arm system. Thus, to obtain high-precision control, the model of the robot (17) is added with the disturbances $\mathbf{d}(\mathbf{q})$ as:

$$\begin{cases} \dot{\mathbf{x}}_1 = \mathbf{x}_2 \\ \dot{\mathbf{x}}_2 = \mathbf{f}_2(\mathbf{q}) + \mathbf{g}_2(\mathbf{q}) \mathbf{T} + \mathbf{d}(\mathbf{q}) \end{cases} \quad (37)$$

where $\mathbf{d}(\mathbf{q})$ denotes the disturbances of the robot model including the model uncertainties $\bar{\mathbf{f}}_2(\mathbf{q})$, $\bar{\mathbf{g}}_2(\mathbf{q})$ and external disturbances \mathbf{D} , yielding:

$$\mathbf{d}(\mathbf{q}) = \bar{\mathbf{f}}_2(\mathbf{q}) + \bar{\mathbf{g}}_2(\mathbf{q}) \mathbf{T} + \mathbf{D}$$

Assumption 1. The state variables \mathbf{q} of the 3-DOF robotic arm driven by EPSS are physically bounded i.e. $|\mathbf{q}| < \mathbf{q}_{max}$, where \mathbf{q}_{max} is constant. The unknown disturbance vector \mathbf{d} varies slowly and is bounded, the disturbances satisfy:

$$|\dot{\mathbf{d}}| \leq \mathbf{d}_{max} \quad (38)$$

where \mathbf{d}_{max} are the constraint constants. Define the estimated disturbance $\hat{\mathbf{d}}$, then estimated error is given by:

$$\tilde{\mathbf{d}} = [\tilde{d}_1 \quad \tilde{d}_2 \quad \tilde{d}_3]^T = \mathbf{d} - \hat{\mathbf{d}} \quad (39)$$

Dynamic equation of estimated disturbance is determined as [24]:

$$\dot{\hat{\mathbf{d}}} = \frac{1}{\varepsilon} (\dot{\mathbf{x}}_2 - \mathbf{f}_2(\mathbf{q}) - \mathbf{g}_2(\mathbf{q}) \mathbf{T} - \hat{\mathbf{d}}(\mathbf{q})) \quad (40)$$

The estimation error dynamics of the disturbance observer is obtained as follows [25]:

$$\dot{\tilde{\mathbf{d}}} = \dot{\mathbf{d}} - \frac{1}{\varepsilon} \tilde{\mathbf{d}} \quad (41)$$

Then,

$$|\tilde{\mathbf{d}}| \leq e^{-(1/\varepsilon)t} |\tilde{\mathbf{d}}(0)| + \varepsilon \rho(t) \quad (42)$$

where $\rho(t)$ denotes an envelope function that $\rho(t) \geq |\dot{\tilde{\mathbf{d}}}|$

Remark 1. Equation (42) shows that the estimated error $\tilde{\mathbf{d}}$ of the nonlinear high-gain disturbance observer can be made arbitrarily small when the observer gain ε is chosen as infinitesimal.

3.2. Robust control design process

In the paper, the complete system including the robot and the EPSS is rendered as a cascade system. Firstly, the system level is taken into account to identify required torque/force to achieve positioning tasks. Subsequently, the control design is carried out at pneumatic actuator level to construct the final control signal. In this step, the nonlinear high-gain disturbance observer is designed to effectively estimate external disturbances acting on the system.

a. The 3-DOF robotic arm control

The conventional backstepping technique is integrated with the sliding mode control to obtain a robust controller for uncertain systems. The basic BSMC for the 3-DOF robotic arm is designed by firstly defining the tracking error as:

$$\mathbf{e}_1 = \mathbf{x}_1 - \mathbf{x}_{1d} \quad (43)$$

where \mathbf{x}_{1d} denotes the desired trajectory. Select Lyapunov candidate function V_1 as:

$$V_1 = \frac{1}{2} \mathbf{e}_1^T \mathbf{e}_1 \quad (44)$$

The time derivative of Equation (44) is taken as follows:

$$\dot{V}_1 = \mathbf{e}_1^T \dot{\mathbf{e}}_1 = \mathbf{e}_1^T (\dot{\mathbf{x}}_2 - \dot{\mathbf{x}}_{1d}) \quad (45)$$

Equation (45) suggests that the virtual control law is chosen as:

$$\mathbf{x}_{2d} = -\mathbf{c}_1 \mathbf{e}_1 + \dot{\mathbf{x}}_{1d} \quad (46)$$

where $\mathbf{c}_1 = \text{diag}(c_{11}, c_{12}, c_{13})$ is a positive definite matrix, then, $\dot{V}_1 \leq 0$. Define a sliding variable $\mathbf{s} = [s_1 \ s_2 \ s_3]^T$:

$$\mathbf{s} = \mathbf{x}_2 - \mathbf{x}_{2d} \quad (47)$$

Subsequently, Lyapunov candidate function V_2 is defined as follows:

$$V_2 = V_1 + \frac{1}{2} \mathbf{s}^T \mathbf{s} \quad (48)$$

The time derivative of equation (48) is taken as

$$\begin{aligned} \dot{V}_2 &= \dot{V}_1 + \mathbf{s}^T \dot{\mathbf{s}} \\ &= -\mathbf{c}_1 \mathbf{e}_1^T \mathbf{e}_1 + \mathbf{s}^T (\mathbf{f}_2(\mathbf{q}) + \mathbf{g}_2(\mathbf{q}) \mathbf{T} + \mathbf{d}(\mathbf{q}) - \dot{\mathbf{x}}_{2d}) \end{aligned} \quad (49)$$

Equation (49) directly indicate that control law \mathbf{T} of the 3-DOF robotic arm is designed as:

$$\mathbf{T}_d = \mathbf{g}_2^{-1}(\mathbf{q}) (-\mathbf{f}_2(\mathbf{q}) - \mathbf{c}_2 \mathbf{s} + \dot{\mathbf{x}}_{2d} - v \text{sgn}(\mathbf{s})) \quad (50)$$

where $\mathbf{c}_2 = \text{diag}(c_{21}, c_{22}, c_{23})$ and $v = \text{diag}(v_1, v_2, v_3)$ are positive definite matrices. Using the estimated disturbance signal (40), Equation (50) is rewritten as follows:

$$\mathbf{T}_d = \mathbf{g}_2^{-1}(\mathbf{q}) (-\mathbf{f}_2(\mathbf{q}) - \mathbf{c}_2 \mathbf{s} + \dot{\mathbf{x}}_{2d} - v \text{sgn}(\mathbf{s}) - \hat{\mathbf{d}}(\mathbf{q})) \quad (51)$$

The control design for the robot level is completed, in the next section, the control action for the EPSS is established.

b. The electro-pneumatic servo system control

The dynamic model of one cylinder is described in detail in subsection 2.3. To calculate the control for the three-cylinder of the robot system, then the equation (35) is rewritten as follows:

$$\dot{\mathbf{F}}_a = \mathbf{f}_a + \mathbf{g}_a \mathbf{u} \quad (52)$$

where $\mathbf{F}_a = [F_{a,1} \ F_{a,2} \ F_{a,3}]^T$, $\mathbf{f}_a = [f_{a,1}(\mathbf{x}, t) \ f_{a,2}(\mathbf{x}, t) \ f_{a,3}(\mathbf{x}, t)]^T$, $\mathbf{u} = [u_1 \ u_2 \ u_3]^T$, and $\mathbf{g}_a = \text{diag}(g_{a,1}(\mathbf{x}, t), g_{a,2}(\mathbf{x}, t), g_{a,3}(\mathbf{x}, t))$, the subscript $n = [1, 2, 3]$ represent the cylinders of the three joints (i.e, shoulder, elbow, and translation joint), respectively.

In order to reduce the influence of parameter uncertainties

of the EPSS, sliding mode control is used for the electro-pneumatic servo control system. Define sliding variable \mathbf{s}_a as follows:

$$\mathbf{s}_a = \mathbf{F}_a - \mathbf{F}_d \quad (53)$$

where \mathbf{F}_d denotes the desired force that determined from the control laws \mathbf{T}_d via the generalized force vectors (11) and the two dynamic force arms (12). Select Lyapunov candidate function V_3 as:

$$V_3 = \frac{1}{2} \mathbf{s}_a^T \mathbf{s}_a \quad (54)$$

The time derivative of equation (54) is taken as:

$$\dot{V}_3 = \mathbf{s}_a^T \dot{\mathbf{s}}_a = \mathbf{s}_a^T (\mathbf{f}_a + \mathbf{g}_a \mathbf{u} - \dot{\mathbf{F}}_d) \quad (55)$$

Based on sliding mode control, the control law \mathbf{u} of electro-pneumatic servo system is designed as follows:

$$\mathbf{u} = \mathbf{g}_a^{-1} (-\mathbf{f}_a - \mathbf{k} \mathbf{s}_a + \dot{\mathbf{F}}_d - \kappa \text{sgn}(\mathbf{s}_a)) \quad (56)$$

where $\mathbf{k} = \text{diag}(k_1, k_2, k_3)$ and $\kappa = \text{diag}(\kappa_1, \kappa_2, \kappa_3)$ are positive definite matrices.

3.3. Stability analysis

Theorem 1. Consider the 3-DOF robotic arm driven by electro-pneumatic servo systems described in general form as equations (17) and (35) under unknown disturbance bounded as Assumption 1, the control laws of the robotic arm (51), the control laws of the EPSS (56), and the observer gains ε of the nonlinear disturbance observer (40) guarantee the Input-to-State Stability [23] of the control system.

Proof of Theorem 1. Lyapunov function candidate is defined as:

$$V = \frac{1}{2} \mathbf{e}_1^T \mathbf{e}_1 + \frac{1}{2} \mathbf{s}^T \mathbf{s} + \frac{1}{2} \tilde{\mathbf{d}}^T \tilde{\mathbf{d}} + \frac{1}{2} \mathbf{s}_a^T \mathbf{s}_a \quad (57)$$

The time derivative of V is taken as:

$$\dot{V} = \mathbf{e}_1^T \dot{\mathbf{e}}_1 + \tilde{\mathbf{d}}^T \dot{\tilde{\mathbf{d}}} + \mathbf{s}^T \dot{\mathbf{s}} + \mathbf{s}_a^T \dot{\mathbf{s}}_a \quad (58)$$

Substituting the control laws (51), (56) and the estimation error dynamic (41) into Equation (58), it can be rewritten as:

$$\begin{aligned} \dot{V} &= -\mathbf{e}_1^T \mathbf{c}_1 \mathbf{e}_1 + \mathbf{s}^T (-\mathbf{c}_2 \mathbf{s} - v \text{sgn}(\mathbf{s}) + \mathbf{d} - \hat{\mathbf{d}}) \\ &\quad + \tilde{\mathbf{d}}^T \left(\dot{\tilde{\mathbf{d}}} - \frac{1}{\varepsilon} \tilde{\mathbf{d}} \right) + \mathbf{s}_a^T (-\mathbf{k} \mathbf{s}_a - \kappa \text{sgn}(\mathbf{s}_a)) \end{aligned} \quad (59)$$

The inequality $|a||b| \geq ab$ is used for Equation (59), thus we obtain:

$$\begin{aligned} \dot{V} &\leq -\mathbf{e}_1^T \mathbf{c}_1 \mathbf{e}_1 - \mathbf{s}_a^T \mathbf{k} \mathbf{s}_a - c_{2i} \left(\frac{s_i}{\zeta_i} - \frac{\zeta_i}{2c_{2i}} \tilde{d}_i \right)^2 \\ &\quad - \tau_i \left(|\tilde{d}_i| - \frac{1}{2\tau_i} |\dot{d}_i| \right)^2 - \left(1 - \frac{1}{\zeta_i^2} \right) c_{2i} s_i^2 - \frac{\eta_i^2}{4c_{2i}} \tilde{d}_i^2 \\ &\quad + \left(\frac{1}{4\tau_i} |\dot{d}_i|^2 \right) \end{aligned} \quad (60)$$

where

$$\tau_i = \left(\frac{1}{\varepsilon} - \frac{\zeta_i^2 + \eta_i^2}{4c_{2i}} \right); \zeta_i > 1; \eta_i \neq 0; i = 1, 2, 3 \quad (61)$$

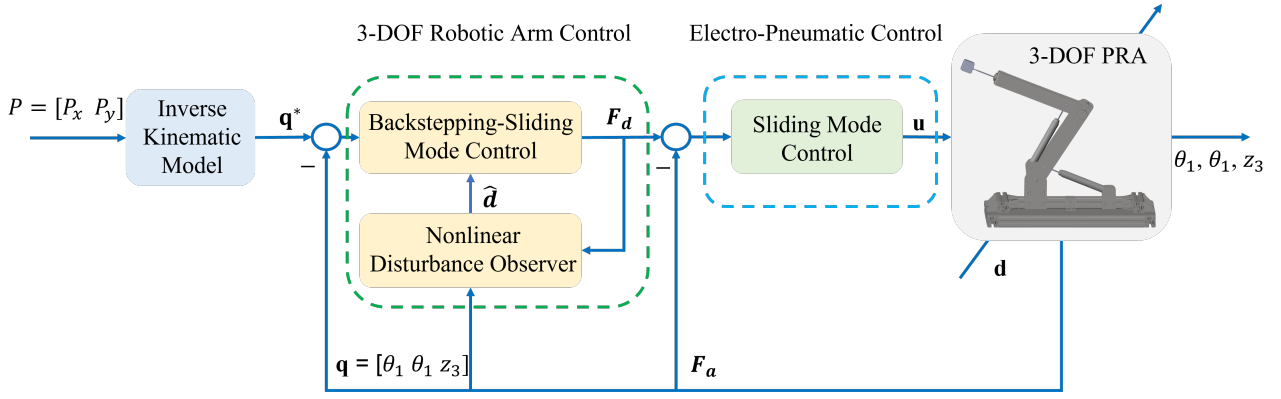


Figure 4: The EPSS actuated 3-DOF robot control structure.

There exists constants ι and γ satisfying the following conditions:

$$\begin{cases} \iota = \sum_{i=1}^3 \left(\frac{1}{4\tau_i} |\dot{d}_i|^2 \right), \\ \gamma = \min \left\{ \left(1 - \frac{1}{\xi_i^2} \right) c_{2i}, c_i, k_i, \frac{\eta_i^2}{4c_{2i}} \right\} \end{cases} \quad (62)$$

Equation (62) can be rewritten as:

$$\dot{V} \leq -2\gamma V + \iota \quad (63)$$

Consequently, it can be concluded that

$$V(t) \leq V(0)e^{-2\gamma t} + \frac{\iota}{2\gamma} (1 - e^{-2\gamma t}) \quad (64)$$

Remark 2. Equation (64) implies that the tracking errors \mathbf{e}_1 , \mathbf{s} , \mathbf{s}_a , and estimation error $\tilde{\mathbf{d}}$ of the 3-DOF robotic arm driven by electro-pneumatic servo systems using the backstepping-sliding mode control with nonlinear high-gain disturbance observer exponentially converge to an arbitrarily tiny ball.

Remark 3. In order to reduce the chattering effect of sliding mode control, the saturation function is used to replace the sign function in the control laws (51), (56).

4. Simulation evaluation

Simulations based on Matlab/Simscape Multibody Link plugin on Solidworks are carried out to demonstrate the control validity of the 3-DOF robotic arm driven by electro-pneumatic servo systems. In which, the electro-pneumatic servo systems are controlled by sliding mode control, and backstepping-sliding mode control with nonlinear high-gain disturbance observer is used for the 3-DOF robotic arm that are shown as in Figure 4. In the simulations, assume that disturbances acting on robot joints is sinusoidal wave form of $0.5 \sin \pi t$ as shown in Figure 11. Parameters of the 3-DOF robotic arm and the proposed controller is expressed in Table 1.

From figures 5, 6, and 7, we can observe that angular and translational motions of the robot under the proposed controller integrated with the disturbances observer exhibit better performances compared to traditional backstepping-sliding mode control. Figures 8, 9, and 10 show that forces produced by the EPSS closely (.i.e. the actual forces) track the desired forces determined by the robot motion control problem. It is also noted that the control forces are well maintained in applicable ranges. The effectiveness of the disturbance observer

Table 1: Parameters of the 3-DOF robotic arm and the proposed controller

Symbol	Value	Unit
m_1	1.335	kg
m_2	0.86	kg
m_f	1	kg
I_1	0.05628	kg · m ²
I_2	0.21154	kg · m ²
$P_1 P_2$	0.3	m
$P_1 P_{m1}$	0.1523	m
$P_2 P_{m2}$	0.165	m
L	0.2	m
P_{atm}	0.1×10^6	Pa
P_s	0.6×10^6	Pa
P_{cr}	0.528	
γ	1.4	
R	287	N · m/kg · K
T	300	K
$\mathbf{c}_1 = \text{diag}(c_{11}, c_{12}, c_{13})$	$\text{diag}(2.5, 2, 4)$	
$\mathbf{c}_2 = \text{diag}(c_{21}, c_{22}, c_{23})$	$\text{diag}(5, 7, 13)$	
$\mathbf{v} = \text{diag}(v_1, v_2, v_3)$	$\text{diag}(1, 2, 1)$	
ε	0.015	

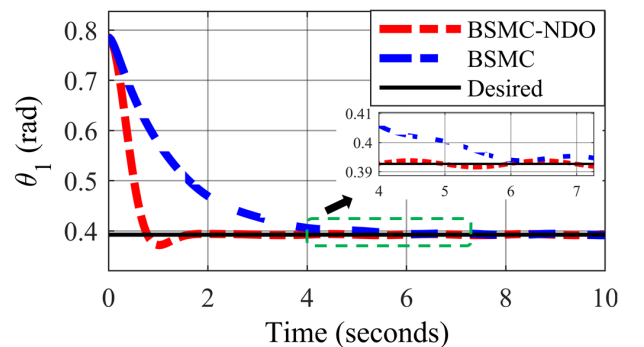


Figure 5: Shoulder joint rotation angle.

is presented in Figure 11, in which the disturbance estimation of the three joints (i.e., shoulder, elbow, and translational joint) follows the disturbances of 3-DOF robotic arm. By using the nonlinear high-gain disturbance observer combined with backstepping-sliding mode control, the rotation angle responses of the shoulder and elbow joints, and translational joint displacement are greatly improved that reducing the in-

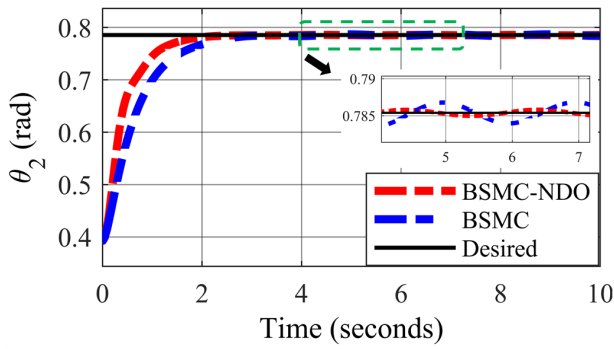


Figure 6: Elbow joint rotation angle.

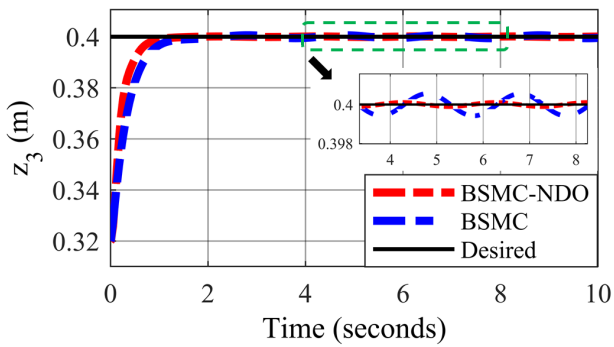


Figure 7: Translational joint displacement.

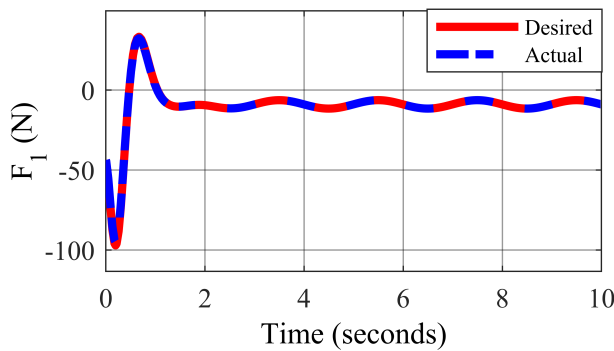


Figure 8: Force response of the pneumatic cylinder F_1 .

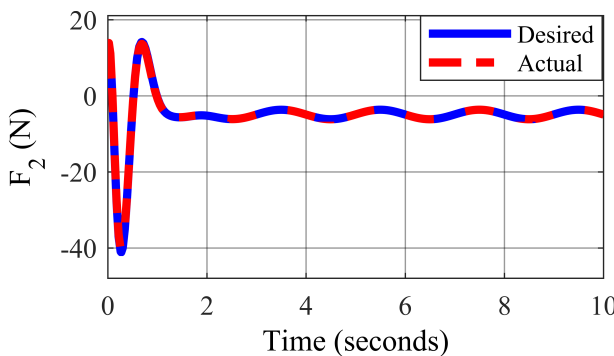


Figure 9: Force response of the pneumatic cylinder F_2 .

fluence of the disturbance of the three joints compared to the conventional backstepping-sliding mode control.

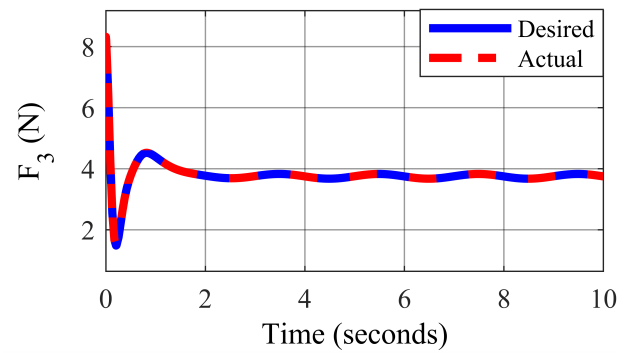


Figure 10: Force response of the pneumatic cylinder F_3 .

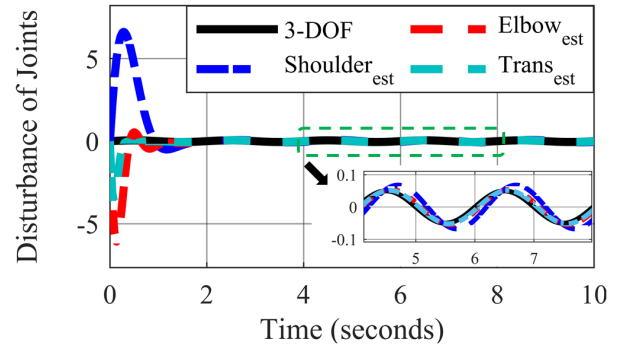


Figure 11: Estimated disturbance responses of robot joints.

5. Conclusion

In the paper, the backstepping-sliding mode control with embedded disturbance is developed for the 3-DOF robot driven by electro-pneumatic actuators. The complicated dynamics of the electro-pneumatic characteristic is considered in the control design. By backstepping-like procedure the control scheme is formulated exhibiting robust property against disturbances. The constructed control allows the system output track the desired signal in a short time period with negligible steady state errors. Currently, the simulation is studied in the paper. In the near future, the experimental results will be presented.

Acknowledgement

Van Trong Dang was funded by Vingroup JSC and supported by the Master, PhD Scholarship Programme of Vingroup Innovation Foundation (VINIF), Institute of Big Data, code VINIF.2021.ThS.26.

References

- [1] Kawakami, Y., Moguchi, H., & Kawai, S. (1990) *Some considerations on the high-speed driving of pneumatic cylinders*. J. Japan Hydraulics & Pneumatics Society, 21(3 May), 318–327.
- [2] Zhijun Li, Shuzhi Sam Ge, Adams, M., & Wijesoma, W. S. (2008) *Adaptive Robust Output-Feedback Motion/Force Control of Electrically Driven Nonholonomic Mobile Manipulators*. IEEE Transactions on Control Systems Technology, 16(6), 1308–1315.
- [3] Dong, W. (2002) *On trajectory and force tracking control of constrained mobile manipulators with parameter uncertainty*. Automatica, 38(9), 1475–1484.
- [4] Yan, Y., Xu, J., & Wiercigroch, M. (2017) *Basins of attraction of the bistable region of time-delayed cutting dynamics*. Physical Review E, 96(3).
- [5] Guo, Q., Zhang, Y., Celler, B. G., & Su, S. W. (2019) *Neural Adaptive Backstepping Control of a Robotic Manipulator with Prescribed Performance Constraint*. IEEE Transactions on Neural Networks and Learning Systems, 30(12), 3572–3583.

- [6] Guo, Q. & Jiang, D. *Nonlinear Control Techniques for Electro-Hydraulic Actuators in Robotics Engineering*. (CRC Press,2017)
- [7] Ali, H., Bahari, S., Noor, M.S., Bashi, S.M., & Marhaban, M.H. (2009) *A Review of Pneumatic Actuators (Modeling and Control)*. Australian Journal of Basic and Applied Sciences, 3 ,pp. 440 - 454.
- [8] Wang, Y.-B & Bao, G. & Wang, Z.-W. (2007) *Application of auto-disturbance rejection controller for pneumatic servo system*. Journal of Dalian Maritime University, Vol 33.
- [9] Zhao, L., Zhang, B., Yang, H., & Li, Q. (2017) *Optimized linear active disturbance rejection control for pneumatic servo systems via least squares support vector machine*. Neurocomputing, 242, 178–186.
- [10] Najjari, B., Barakati, S. M., Mohammadi, A., Futohi, M. J., & Bostanian, M. (2014) *Position control of an electro-pneumatic system based on PWM technique and FLC*. ISA Transactions, 53(2), 647–657.
- [11] Karpenko, M., & Sepehri, N. (2004) *QFT design of a PI controller with dynamic pressure feedback for positioning a pneumatic actuator*. Proceedings of the 2004 American Control Conference.
- [12] Parnichkun, M., & Ngaecharoenkul, C. (2001) *Kinematics control of a pneumatic system by hybrid fuzzy PID*. Mechatronics, 11(8), 1001–1023.
- [13] Smaoui, M., Brun, X., & Thomasset, D. (2006) *A study on tracking position control of an electropneumatic system using backstepping design*. Control Engineering Practice, 14(8), 923–933.
- [14] Ren, H.-P., Wang, X., Fan, J.-T., & Kaynak, O. (2019) *Adaptive Backstepping Control of a Pneumatic System With Unknown Model Parameters and Control Direction*. IEEE Access, 7, 64471–64482.
- [15] Ren, H.-P., & Huang, C. (2013) *Adaptive backstepping control of pneumatic servo system*. 2013 IEEE International Symposium on Industrial Electronics.
- [16] Carneiro, J. F., & de Almeida, F. G. (2014) *Accurate motion control of a servopneumatic system using integral sliding mode control*. The International Journal of Advanced Manufacturing Technology, 77(9-12), 1533–1548.
- [17] Blagojević, V., Šešlija, D., Stojiljković, M. & Dudić, S. Efficient control of servo pneumatic actuator system utilizing by-pass valve and digital sliding mode. *Sadhana*, **38**, 187-197 (2013)
- [18] Tran, X., Nguyen, V., Nguyen, N., Pham, D. & Phan, V. Sliding mode control for a pneumatic servo system with friction compensation. *International Conference On Engineering Research And Applications*. pp. 648-656 (2019)
- [19] Liu, G., Li, G., Song, H. & Peng, Z. Neural network sliding mode control for pneumatic servo system based on particle swarm optimization. *Proceedings Of The 11th International Conference On Modelling, Identification And Control (ICMIC2019)*. pp. 1239-1248 (2020)
- [20] Plestan, F., Shtessel, Y., Brégeault, V., & Poznyak, A. (2010) *New methodologies for adaptive sliding mode control*. International Journal of Control, 83(9), 1907–1919.
- [21] Ren, H., & Fan, J. (2016) *Adaptive backstepping slide mode control of pneumatic position servo system*. Chinese Journal of Mechanical Engineering, 29(5), 1003–1009.
- [22] Lu, C.-H., Hwang, Y.-R., & Shen, Y.-T. (2010) *Backstepping Sliding-Mode Control for a Pneumatic Control System*. Proceedings of the Institution of Mechanical Engineers, Part I: Journal of Systems and Control Engineering, 224(6), 763–770.
- [23] Sontag, E. Input to state stability: Basic concepts and results. *Nonlinear And Optimal Control Theory*. pp. 163-220 (2008)
- [24] Dang, V., Le, D., Nguyen-Thi, V., Nguyen, D., Tong, T., Nguyen, D., Nguyen, T. & Others Adaptive Control for Multi-Shaft with Web Materials Linkage Systems. *Inventions*, **6**, 76 (2021)
- [25] Le, D., Nguyen, D., Le, N. & Nguyen, T. Traction control based on wheel slip tracking of a quarter-vehicle model with high-gain observers. *International Journal Of Dynamics And Control*. pp. 1-8 (2021)